FUNCTION™ american physiological society

FUNCTION, 2022, 3(5): zqac042

https://doi.org/10.1093/function/zqac042
Advance Access Publication Date: 24 August 2022
Original Research

RESEARCH ARTICLE

Deletion of Mechanosensory β1-integrin From Bladder Smooth Muscle Results in Voiding Dysfunction and Tissue Remodeling

Weiqun Yu[1], Bryce MacIver[1], Lanlan Zhang[1,§], Erica M. Bien[1], Nazaakat Ahmed[1], Huan Chen[1,#], Sarah Z. Hanif[1], Mariana G. de Oliveira[2], Mark L. Zeidel[1], Warren G. Hill[1,*]

[1]Laboratory of Voiding Dysfunction, Nephrology Division, Department of Medicine, Beth Israel Deaconess Medical Center and Harvard Medical School, Boston, MA 02215, USA and [2]Department of Pharmacology, Faculty of Medical Sciences, University of Campinas (UNICAMP), Campinas, SP 13083-970, Brazil

*Address correspondence to W.G.H. (e-mail: whill@bidmc.harvard.edu)

§Present address: Division of Pulmonary Diseases, State Key Laboratory of Biotherapy of China, and Department of Respiratory Medicine, West China Hospital of Sichuan University, Chengdu, China
#Present address: The School of Basic Medical Sciences, Southwest Medical University, Luzhou, Sichuan, China

Abstract

The bladder undergoes large shape changes as it fills and empties and experiences complex mechanical forces. These forces become abnormal in diseases of the lower urinary tract such as overactive bladder, neurogenic bladder, and urinary retention. As the primary mechanosensors linking the actin cytoskeleton to the extracellular matrix (ECM), integrins are likely to play vital roles in maintaining bladder smooth muscle (BSM) homeostasis. In a tamoxifen-inducible smooth muscle conditional knockout of β1-integrin, there was concomitant loss of α1- and α3-integrins from BSM and upregulation of αV- and β3-integrins. Masson's staining showed a reduction in smooth muscle with an increase in collagenous ECM. Functionally, mice exhibited a changing pattern of urination by voiding spot assay up to 8 wk after tamoxifen. By 8 wk, there was increased frequency with reductions in voided volume, consistent with overactivity. Cystometrograms confirmed that there was a significant reduction in intercontractile interval with reduced maximal bladder pressure. Muscle strip myography revealed a loss of contraction force in response to electrical field stimulation, that was entirely due to the loss of muscarinic contractility. Quantitative western blotting showed a loss of M3 receptor and no change in $P2X_1$. qPCR on ECM and interstitial genes revealed loss of Ntpd2, a marker of an interstitial cell subpopulation; and an upregulation of S100A4, which is often associated with fibroblasts. Collectively, the data show that the loss of appropriate mechanosensation through integrins results in cellular and extracellular remodeling, and concomitant bladder dysfunction that resembles lower urinary tract symptoms seen in older people.

Submitted: 13 June 2022; **Revised:** 12 August 2022; **Accepted:** 15 August 2022

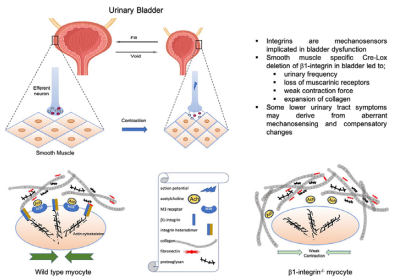

Key words: cell adhesion; mechanotransduction; LUTS; acetylcholine; cholinergic; phenotypic conversion

Introduction

Integrins are a family of proteins that are universally expressed in all cells and play important roles as both cell adhesion molecules and mechanosensors.[1,2] While universal, isoforms are expressed in different patterns in different tissues thus generating a broad range of functional diversity. Located at the plasma membrane and spanning the membrane, they bind to extracellular matrix (ECM) molecules on the cell exterior, as well as to the actin cytoskeleton on the interior. Their binding affinity on both sides of the membrane is continuously modulated by mechanical stimuli and by intracellular signals. In the face of physical forces that deform cell shape such as in blood vessels that experience pulsatile flow, they can reinforce the membrane dynamically through formation of multiprotein complexes called focal adhesions. Focal adhesions, in turn, recruit and remodel the actin cytoskeleton as well as ECM components such as fibronectin and collagens, to maintain homeostasis or respond to injury.

The urinary bladder is a highly distensible hollow organ as well as a mechanically efficient pump in which the work is performed by the bladder smooth muscle (BSM). Its activity is characterized by periodic stretching/elongation due to filling and then contraction to expel urine, with each phase having very different time signatures. After slow filling, surface area expansion, and muscle elongation, wall stretch leads to sensory afferent firing and higher centers in the brain (ie, the pontine micturition center and periaqueductal gray), coordinate the decision to void.[3,4] The bladder therefore exhibits sophisticated mechanosensory mechanisms that regulate accommodation during filling, but which then can rapidly switch to mechanotransduction pathways that facilitate smooth muscle (SM) contraction to achieve the rapid voiding phase.

The bladder however, is prone to storage and micturition problems leading to a spectrum of lower urinary tract symptoms (LUTS), which can range from the mildly inconvenient to the incapacitating. LUTS include voiding, storage, obstructive, and irritative symptoms and are a significant problem for tens of millions of people in the United States.[5] Worldwide prevalence estimates for all major LUTS categories suggest that over 4.3 billion people are affected.[6] As well as the physical discomfort, isolation, and pain, these pathologies often produce attendant and adverse emotional and psychological symptoms (eg, anxiety and depression), which significantly impact quality of life for sufferers. The underlying causes for many of these benign problems of the lower urinary tract are unknown, and clinically, the goal is usually symptomatic relief through modifying the mechanics of voiding, usually by inhibiting SM contractility (anticholinergics and botulinum neurotoxin) or by enhancing relaxation (beta agonists).[7] This places SM squarely as the initial point of therapeutic focus in many forms of LUTS.

In efforts to understand the molecular and physiological changes that accompany a common bladder injury, we recently characterized an acute urinary retention (AUR) model in mice, that recapitulated important aspects of AUR in humans.[8] Following transurethral catheterization and a 30-min exposure of the bladder to 50 and 80 cm H_2O pressure, there was a clear evidence of bladder dysfunction at 24 h, with a loss of contractility. There was also a rapid upregulation within 6 h of the expression of β1-integrin and several important focal adhesion adaptor proteins, including talin and paxillin, as well as the integrin-dependent kinases, focal adhesion kinase, and integrin-linked kinase. These data pointed directly to the involvement of integrins in mediating stretch-mediated injury responses. Therefore to test the hypothesis that integrins represent primary mechanosensors in the BSM, we engineered the deletion of β1-integrin from adult SM in mice, through induction of Cre recombinase in response to tamoxifen (TMX). Data from these tissue-conditional knockouts strongly implicate integrin participation in multiple aspects of voiding and of regulating processes from BSM contraction to matrix remodeling.

Materials and Methods

Chemicals: TMX was from MP Biomedicals (Irvine, CA, USA) and all other chemicals were from Sigma (St. Louis, MO, USA) unless otherwise specified.

Mice: A TMX-inducible SM-conditional knockout mouse for β1-integrin was generated for this study by crossing B6.FVB-Tg(Myh11-cre/ERT2)1Soff/J mice with B6;129-*Itgb1*^{tm1Efu}/J, beta1-integrin floxed mice (The Jackson Laboratory; Bar Harbor, ME, USA). The Cre-engineered strain expresses Cre recombinase in the presence of TMX and under control of the SM myosin heavy chain 11 polypeptide promotor (*Myh11*). Due to the Y chromosome insertion of the SMMHC-CreER^{T2} transgene, expression of Cre is restricted to males only and so all data presented are from male mice. All mouse experiments were performed in accordance with an animal protocol approved by the Beth Israel Deaconess Medical Center Institutional Animal Care and Use Committee (IACUC), which is AALAC accredited and adheres to international standards of animal welfare.

TMX-induction of mice: At 12–16 wk of age, conditional-knockout mice (Myh11$^{\beta 1\text{-}fl/fl}$) were i.p. injected with 2 mg TMX (20 mg/mL stock solution dissolved in corn oil) for 5 consecutive days. Controls were genetically identical littermates injected with corn oil vehicle. TMX-induced mice began dying 8 wk postinjection and exhibited gross gut distension, presumably as a result of the loss of β1-integrin from gastrointestinal SM. Therefore, most phenotypic and molecular analyses were performed at 6 wk at which point mice appeared active and healthy.

Genotyping: Genomic DNA was extracted from mouse tail snips using a modification of the HotSHOT method.[9] Tail tissues were incubated in 500 μL 50 mM NaOH for 15 min followed by an addition of 55 μL 1 M Tris-HCl pH 7.2 to neutralize, then aliquots (2–3 μL) were used for polymerase chain reaction (PCR). Extracted DNA was stored at −20°C. Genotyping primer sequences and thermal cycling conditions for Myh11-cre were provided by Jackson Laboratory and were 12 026 5′-TGA CCC CAT CTC TTC ACT CC-3′ and 12 028 5′-AGT CCC TCA CAT CCT CAG GTT-3′, forward and reverse, respectively, for Cre, and oIMR7338 5′-CTA GGC CAC AGA ATT GAA AGA TCT-3′ and oIMR7339 5′-GTA GGT GGA AAT TCT AGC ATC ATC C-3′, forward and reverse, respectively, as a positive control. Primer sequences to detect β1-integrin were also provided by Jackson Laboratory and were 5′-CGG CTCA AAG CAG AGT GTC AGT C-3′ and 5′-CCA CAA CTT TCC CAG TTA GCT CTC-3′, forward and reverse, respectively. Thermal cycling conditions for detecting β1-integrin genotypes were initial denature 94°C for 3 min, cycling denature 94°C for 30 s, anneal 65°C for 60 s, extend 72°C for 60 s, 35 cycles. New England Biolabs (Danvers, MA, USA) 5× Taq master mix was used for genotyping PCR. Products were electrophoresed on 1% agarose gels, stained with ethidium bromide and visualized under UV light.

qPCR—RNA extraction: Mice were euthanized by CO_2 inhalation and the bladder quickly removed to a silicone-coated dish on ice with cold phosphate buffered saline (PBS). Bladders were cut open from urethra to dome and pinned flat before the detrusor and urothelial/mucosal layers were carefully separated by peeling. Detrusor tissue was then added to tubes of 2 mm ceramic BashingBeads (Zymo, Irvine, CA, USA) containing 700 μL Trizol (Invitrogen, Carlsbad, CA, USA) and given 2 × 30 s shakes at 5 m/s on a Fisher Scientific Bead Mill (Waltham, MA, USA) to completely disrupt the tissue. The Trizol solution was transferred to a new 1.5 mL tube and 140 μL chloroform was added to initiate phase separation by vigorous hand mixing then centrifugation. The aqueous phase was transferred to a new 1.5 mL tube and total RNA was precipitated with isopropanol followed by centrifugation and then washing with 70% (v/v) ethanol. The RNA pellet was air dried, then dissolved in water. The Bashing Beads can leave small fines, which disrupt quantification so the RNA was further purified through Qiagen (Germantown, MD, USA) RNeasy Plus columns following manufacturer's instructions, and includes a step that results in DNA removal. Total RNA was quantified by spectrophotometry.

qPCR—reverse transcription: Invitrogen's Superscript IV First-Strand Reverse Transcription Kit was used following the manufacturer's instructions. The resulting reaction was normalized to the measured amount of total RNA used by diluting to the equivalent of 10 ng/μL total RNA. qPCR was carried out on a Quantstudio 6 Flex (Applied Biosystems, Bedford, MA, USA) using triplicate reactions for each gene of interest (GOI) in 15 μL volumes per well. Thermo Fisher (Waltham, MA, USA) Maxima Sybr Green reagents were used. All experiments included melt curves to monitor reaction integrity.

Western blotting: Rabbit antibodies to β1-integrin (ab52971), and muscarinic receptor 3 (M3, ab126168) were from Abcam (Waltham, MA, USA); α1-integrin (#71 747), β3-integrin (#13 166), and β-actin (#4697) were from Cell Signaling Technology (Danvers, MA, USA); M2 (G206) was from Assay Biotech (Fremont, CA, USA) and $P2X_1$ (APR001) was from Alomone Laboratories (Jerusalem, Israel). Detrusor tissue was lysed in RIPA buffer (150 mM NaCl, 50 mM Tris, 1% (v/v) NP40, 0.5% deoxycholic acid, and 1% SDS, pH 7.4) containing protease inhibitors (Complete Mini). Samples were loaded at 25 μg protein/lane on NuSep 8–16% SDS polyacrylamide gels (Germantown, MD, USA) and separated by SDS-PAGE prior to electrotransfer to Immun-Blot PVDF (Bio-Rad, Hercules, CA, USA). Membranes were blocked in 5% milk powder/tris buffered saline (TBS) for 1 h prior to overnight incubation in primary antibodies (1:1000 in TBS/0.05% (v/v) Tween 20) at 4°C. Following washing and secondary antibody incubation (1:10,000 in TBS/0.05% (v/v) Tween 20), binding was detected with an Amersham ECL kit and exposure to film. Blots were always stripped with OneMinute Plus stripping buffer (GM Biosciences, Frederick, MD, USA) and then reprobed with β-actin antibody for internal normalization of loading. Band densities were quantitated using FIJI version of Image J (method described at: https://lukemiller.org/index.php/2010/11/analyzing-gels-and-western-blots-with-image-j/).

Immunofluorescence: Opened and pinned excised bladders were fixed in 4% paraformaldehyde/PBS for 2 h at room temperature and then washed into PBS. Fixed tissues were cryoprotected in 30% sucrose (w/v)/PBS for ∼2 h, frozen in OCT and sectioned onto slides before incubation in rat antimouse β1-integrin antibody (1:100, #550 531, BD Biosciences) at 4°C overnight. Sections were then incubated with Alexa Fluor 488-conjugated secondary antibody (1:100) and nuclei counterstained with DAPI (4′,6-diamidino-2-phenylindole). Images were obtained on an Olympus BX60 fluorescence microscope with a 40× objective (1600 × 1200 pixels) using cellSens software.

Histology: Whole excised bladders were fixed in 4% paraformaldehyde/PBS overnight at 4°C overnight and then washed into PBS. Paraffin embedding, sectioning in cross-section and Masson's trichrome staining were performed by the BIDMC Histology Core Facility. Imaging was done on the same microscope as for immunofluorescence. Quantitation of images in terms of blue and red areas (for collagen and SM, respectively) was performed with Image J through color deconvolution and using the Masson's trichrome vector setting. Multiple random regions of interest (ROIs) of defined size were placed on several images and quantitated for area% following thresholding of the separated blue and red color images.

Cystometrograms (CMG): CMGs were performed under urethane anesthesia (1.3 g/kg) with continuous infusion of PBS through the dome of the bladder at 25 μL/min, as previously described in detail.[8]

Void spot assay (VSA): VSAs were performed as described previously.[8,10,11] Mice were moved individually to empty mouse cages with precut filter paper (Blicks Cosmos blotting paper #10422–1005) on the bottom. They were provided with food in the usual wire racks, but no water. After 4 h, mice were returned to their home cages and the filter paper allowed to dry before being photographed under UV light (365 nm) in a Chromato-Vue C75 imaging box with on board Canon camera (EOS Rebel T3–12 megapixels). During image analysis, many overlapping spots were outlined with the drawing tool in the Fiji version of Image J, copied, and moved to an empty area of the filter. Void spot areas were quantitated using UrineQuant software.

Myography: Myography and electrical field stimulation (EFS) of mucosa-dissected bladder muscle strips were performed in SI-MB4 organ baths (World Precision Instruments, Sarasota, FL, USA) as described in detail previously.[8,10]

Data/Statistical analysis: This study was exploratory in nature rather than strictly hypothesis-driven with a predetermined study design, group sizes, etc., as defined in Michel et al. (2020).[12] Consequently, all *P* values based on statistical testing should be considered descriptive. Minimum group sizes of 4 mice/genotype or treatment (TMX or vehicle) were employed for all assays with the exception of western blotting and

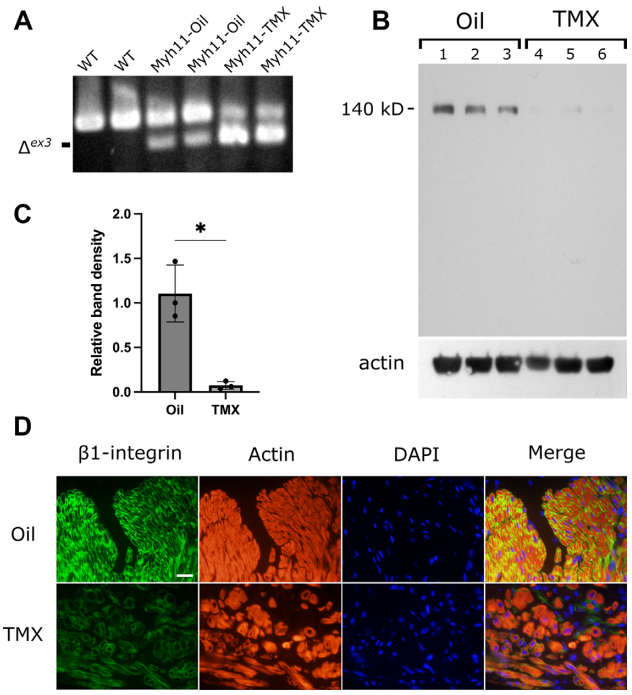

Figure 1. Characterization of the mouse model. (A) RT-PCR of β1-integrin from detrusor extracted mRNA at 6 wk after i.p. injections. Expression of functional Cre in β1-integrin floxed mice is evidenced by a smaller DNA product lacking exon 3 (Δ^{ex3}), which is not present in wild type mice. Myh11$^{\beta 1\text{-}fl/fl}$ mice were induced with TMX or injected with corn oil vehicle (Myh11-TMX and Myh11-Oil, respectively). (B) Western blotting of β1-integrin in detrusor from oil- and TMX-injected mice at 6 wk after injections. β-actin loading controls are shown in the lower panel. (C) Quantitation of densitometry from (B) normalized to the amount of actin in each lane. Data are mean ± SD, $*P < 0.05$, based on t-test with Welch's correction for unequal variances. (D) Immunofluorescence of β1-integrin in BSM of oil- and TMX-injected Myh11$^{\beta 1\text{-}fl/fl}$ mice (left panels, green). Phalloidin staining shows actin (red) and DAPI highlights nuclei (blue). Scale bar (white) in top left panel = 10 μm.

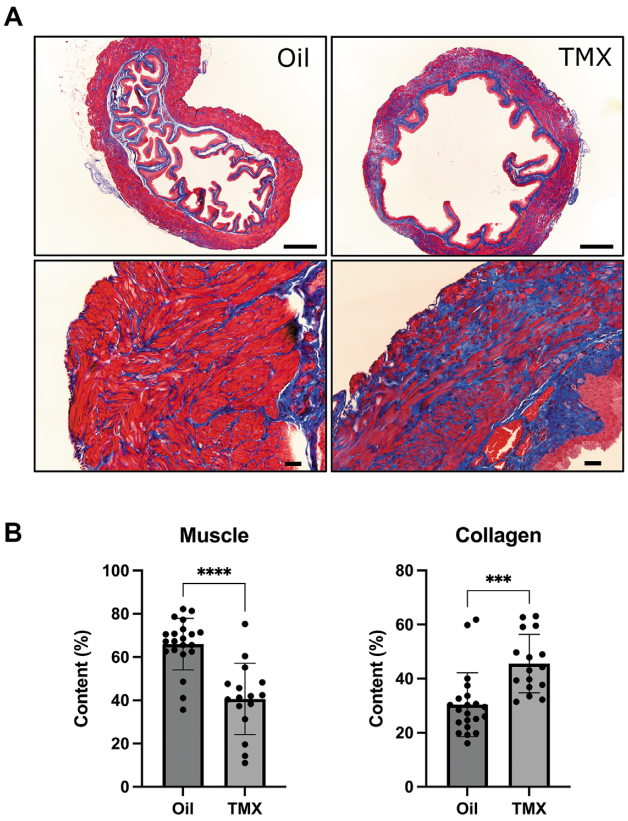

Figure 2. (A) Masson's trichrome staining of whole bladder sections from oil- and TMX-injected mice at 6 wk after induction shows deposition of collagenous ECM (blue) and loss of SM (red) in detrusor upon loss of β1-integrin. Upper and lower panels taken with 4× and 20× objectives, and scale bars are 200 and 20 μm, respectively. (B) Quantitation of color deconvoluted images in red and blue channels on multiple ROIs randomly placed on images of 2 bladders for each treatment. Data are mean ± SD, *** $P < 0.001$, **** $P < 0.0001$ by unpaired t-test.

immunofluorescence, where n's of 3 from a single experiment are presented. Experiments with different groups of TMX-induced and control mice were always performed at least twice.

Results

Characterization of Myh11$^{\beta 1\text{-}fl/fl}$ Mice

Upon successful crossing of the Cre and floxed mouse lines, we characterized the resulting Myh11$^{\beta 1\text{-}fl/fl}$ offspring. Figure 1A shows the results of RT-PCR on mRNA extracted from detrusor that had been separated by carefully peeling away the muscosal layer. In both uninduced controls (injected with corn oil vehicle), and TMX-induced littermates, Myh11$^{\beta 1\text{-}fl/fl}$ bladders showed evidence of a smaller transcript lacking exon 3 (Δ^{ex3}). The amount of this transcript was greatly enhanced with TMX-induction demonstrating that Cre expression was significantly upregulated upon binding of TMX to the mutant estrogen receptor element fused to Cre. It also showed that there was some "leakage" of expression occurring in the absence of induction. The presence of some full length β1-integrin transcript after TMX-induction was not unexpected as detrusor contains cell types other than SM (eg, interstitial, immune, neural, etc.), and in these Cre expression would be absent, and therefore full-length integrin present.

Bladders taken from Myh11$^{\beta 1\text{-}fl/fl}$ mice 6 wk after induction or vehicle injection (corn oil) were analyzed by western blotting for β1-integrin protein. As seen in Figure 1B and C, there was greater than 90% reduction in its expression, demonstrating a convincing inducible knockout. Immunofluorescence staining further supported the loss of β1-integrin from adult detrusor (Figure 1D).

Loss of BSM β1-integrin Results in Detrusor Remodeling

To determine whether the loss of β1-integrin would alter BSM morphology, we performed histology with Masson's trichrome staining (Figure 2). This showed striking evidence of large-scale tissue remodeling, with an apparent loss of SM content (red) and an expansion of extracellular collagenous matrix (blue). In the integrin knockouts, there was also disruption to the organized packing of muscle bundles in the detrusor. Bladder and body weights between C57BL6/J's, vehicle and knockout groups were however, not different (data not shown). A color deconvolution analysis of multiple ROI's chosen to randomly cover two entire bladders/group revealed highly significant remodeling of the detrusor in mice lacking β1-integrin (Figure 2B).

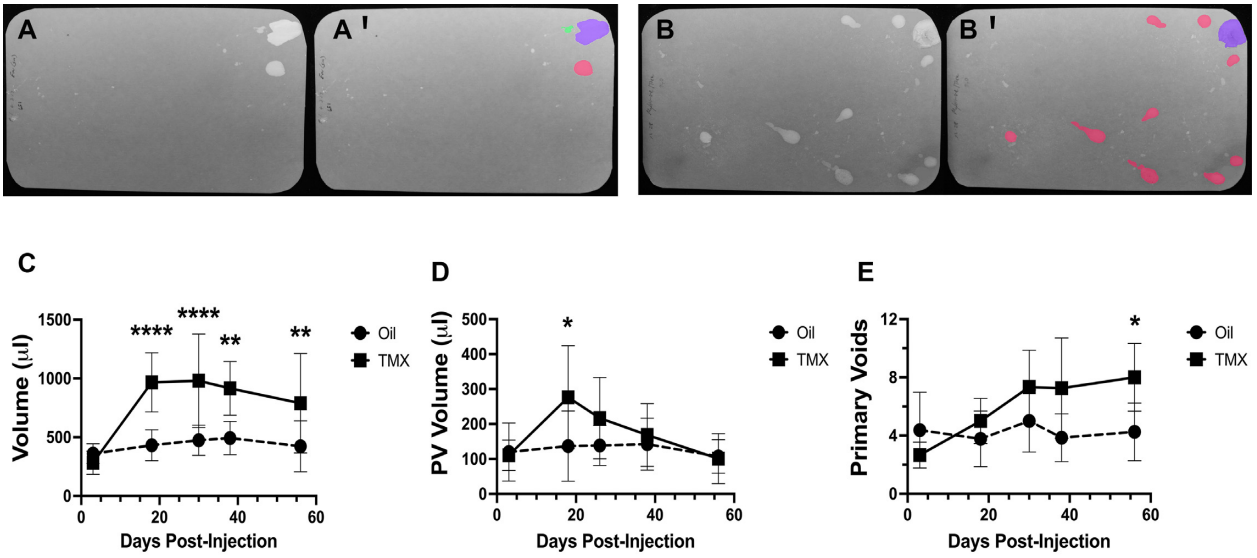

Figure 3. VSAs show changing micturition parameters over time in TMX-induced Myh11$^{\beta 1\text{-}fl/fl}$ mice. (A and B) Void spot filter papers imaged under UV light. (A′ and B′) Automated spot detection of (A) and (B) by UrineQuant software with pseudocoloring. Purple represents voids >100 μL, red shows spots between 20 and 100 μL, with green less than 20 μL and greater than 1 μL. Purple and red collectively represent PVs, which are defined as >20 μL in volume. Images are from mice at day 56 after injections, with (A) being oil-injected and (B) TMX-injected. (C–E) Summary data (mean ± SD) from repeated void spot testing on the same groups of mice ($n = 8$ and 9 for oil and TMX mice, respectively). Significance was tested by 2-way ANOVA with between-treatment multiple comparisons by Sidak's test. * $P < 0.05$, ** $P < 0.01$, **** $P < 0.0001$. (C) Total urine volume, (D) mean PV volume, and (E) number of PV's.

Void Pattern Changes Suggest Voiding Dysfunction

To see how these changes might impact the normal voiding behavior of Myh11$^{\beta 1\text{-}fl/fl}$ mice, we performed longitudinal VSAs on 8 control and 9 TMX-induced knockouts. Since the assay is noninvasive, the same mice were followed at set intervals out to 56 days, and changes in voided volumes, number of voiding events, and total volumes, quantitated and compared. Figure 3A and B shows examples of filter papers from control and TMX-induced mice, respectively (at day 56), following 4 h of normal conscious behavior and voluntary micturition. The corresponding images in Figure 3A′ and B′ are the pseudocolored representations following spot detection by UrineQuant software. We have determined from previous in-depth characterization of voiding behavior using this assay that there is a volume cutoff at ~20 μL that distinguishes a "real" or "primary" void (PV) from other incidental spotting.[13] The "incidental" spotting is typically less than 2.5% of the total volume voided in healthy young mice. PV parameters therefore capture important elements of the urinary tract physiology in a model. In Figure 3A′ and B′, red and purple spots are PVs and there are significantly more present in the TMX-induced mouse (Figure 3B′).

Figure 3C, D, and E provides the summarized data for total urine volume, number of PVs, and mean PV volume, respectively. The most obvious feature is the dramatic increase in total voided urine in TMX-treated mice (Figure 3C), which is evident by day 18 and is then maintained for the remaining life span of these mice. While dramatic, this is likely to reflect phenomena related to volume homeostasis, including drinking, vascular and gut permeability, and ureter function, rather than a bladder phenotype. Each of these other SM containing organs will also experience the loss of β1-integrin and it appears at least one consequence is the production of more urine. More interestingly, we see a slow increase in the number of PVs, which roughly double from 4 to 8 (Figure 3E), and which peak at day 56 ($P < 0.05$), while simultaneously there is a changing pattern in terms of the average voided volume (Figure 3D). Here, the volume/void becomes significantly larger at day 18 ($P < 0.05$) consistent with the overall early increase in urine (Figure 3C) but then diminishes back to baseline by day 56. This occurs despite the total voided urine staying very high throughout (Figure 3C). An increase in number of voids and a decrease in the volume/void suggests some degree of overactivity.

Cystometry Demonstrates Increased Reflex Micturition Frequency With Reduced Contractile Pressure

We next examined the urodynamic characteristics of these mice by cystometry under urethane anesthesia (Figure 4). Figure 4A and B shows characteristic intrabladder pressure tracings during continuous filling (25 μL/min), of control (Figure 4A) and TMX-injected (Figure 4B) mice. It is clear that the intervals between voids (rapid pressure spikes) are much shorter in the integrin-deficient mice and the peak pressures generated are lower. Comparisons of summary data for 5 different parameters in both groups, are shown in Figure 4C–G. Peak pressures (defined as peak—baseline pressure) were significantly lower and the intercontractile intervals were significantly shorter. The bladder compliance was not significantly different (Figure 4E), but suggestively, tended to be lower in knockouts, and both baseline pressures (postvoiding) and micturition pressure thresholds (Figure 4F) were higher in the bladders lacking SM integrin β1.

Reduced Detrusor Contractility by Myography

VSA's indicated that ultimately the conditional knockout mice void more frequently with smaller volumes/void, and cystometry provided additional evidence for increased frequency/overactivity. It also suggested some deficit in contractile force generation. We therefore used muscle strip myography to interrogate the force generating ability of β1-integrin deficient

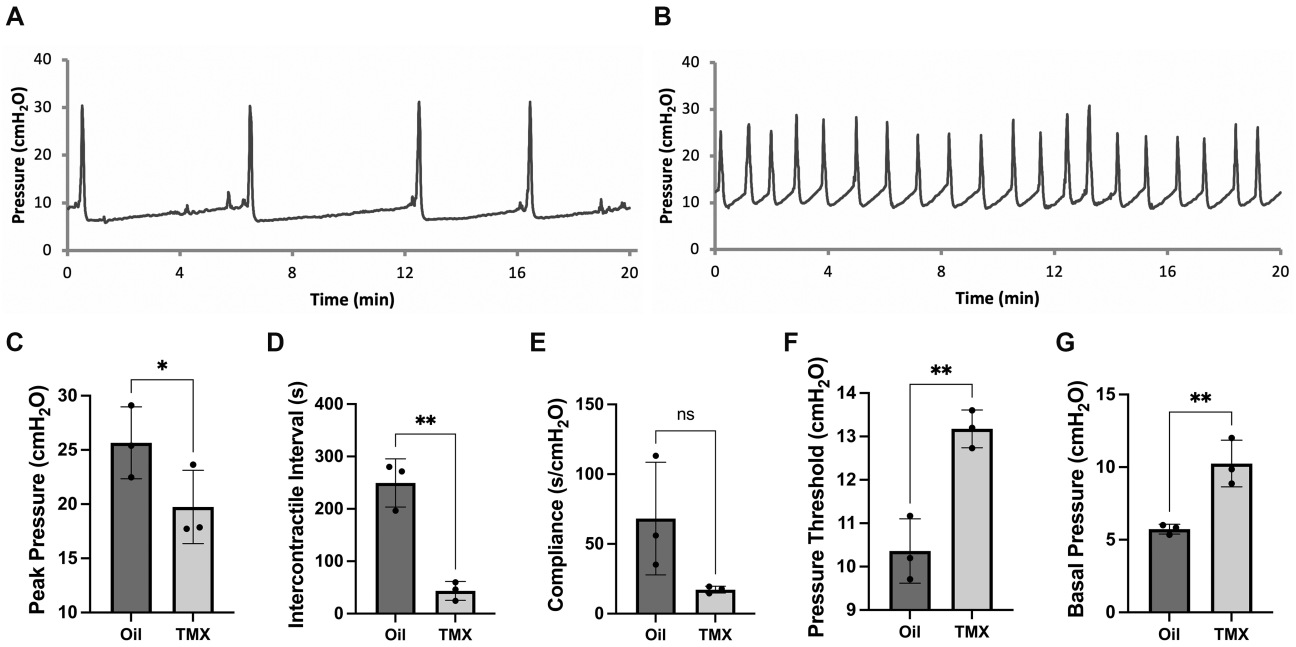

Figure 4. Cystometry under urethane anesthesia demonstrates that the loss of β1-integrin from BSM causes increased frequency of voiding and loss of contractile force. Intrabladder pressure tracings during continuous filling at 25 μL/min in (A) an oil-injected mouse and (B) a TMX-injected mouse at 6 wk. (C–G) Summary data from 4 mice/group showing means ± SD (C) Peak pressure—baseline pressure, (D) intercontractile intervals, (E) compliance during the filling phase, (F) pressure threshold at which a voiding contraction initiates, and (G) baseline pressure following completion of voiding. $*$ $P < 0.05$, $**$ $P < 0.01$, ns—not significant.

SM (Figure 5). Figure 5A and B (tracings at left) shows representative responses to EFS by control and TMX-induced bladder strips, respectively. Loss of β1-integrin dramatically reduced the force that the BSM was able to generate (Figure 5B compared to 5A) consistent with cystometric data. To define whether there was a specific loss of cholinergic or purinergic contractile signaling, we used atropine to inhibit muscarinic acetylcholine receptors. Figure 5A and B (tracings at right) shows that in control bladder approximately 60% of force was inhibitable with atropine. In integrin knockout tissue however (Figure 5B), atropine had very little effect. Quantitation of EFS responses of multiple strips from several mice/group is shown in Figure 5C. Contraction force in the TMX-induced bladders was severely curtailed (third set of boxes) and was of a similar magnitude to control bladders treated with atropine (second set of boxes). Atropine treatment of integrin deficient muscle showed no significant difference in contraction force, which demonstrated that the loss of β1-integrin had selectively impacted cholinergic signaling while sparing the purinergic signaling pathway.

Muscarinic Receptor Downregulation

To shed light on what this regulatory interaction might entail, we ran western blots and qPCR on 2 major muscarinic receptors known to be expressed in BSM (M2 and M3) and on the major purinergic receptor, $P2X_1$ (Figure 6). M3, which is known to be the dominant functional acetylcholine receptor in BSM,[14] was significantly down-regulated in TMX-induced mice (Figure 6B). M2 tended to be lower in these animals as well (Figure 6A), while P2 × 1 was unchanged (Figure 6C). To perform qPCR, we quantitated expression levels of 3 control genes (*sdha*, *actb*, and *ywhaz*), averaged them for threshold cycle number (mean value 22.3 for 8 mice), then subtracted the GOI cycle number to obtain deltaCt values (dCt). Quantitation of transcript levels by this technique confirmed the protein expression data (Figure 6D) with lower dCt values indicating less expression.

Compensatory Changes in Integrin Expression

Since functional integrins at the plasma membrane are heterodimers consisting of both an alpha and a beta subunit, we were curious as to whether the genetic ablation of a single integrin would have an impact on other integrin isoforms and hence on the ability to construct focal adhesions. Western blotting for two of the other most highly expressed integrins in BSM[15] showed that expression of α1-integrin was significantly downregulated (Figure 7A), while β3-integrin was upregulated in TMX-induced mice (Figure 7B). In the case of α1-integrin, the loss of its cognate monomer presumably leads to a feedback downregulation in expression, while for β3, there may be a compensatory upregulation. These data imply a dramatic restructuring of cell and focal adhesions in this tissue. Gene expression levels of these and other integrins were examined by qPCR (Figure 7C). This analysis provided some interesting information on the relative expression levels of multiple integrins that have previously been described in bladder, with α4-integrin having very low expression while β1 and α5 were highest. α1- and α3-integrin were both seen to be significantly downregulated in β1-null muscle, while αV was upregulated. Interestingly, β3 mRNA levels were not different, thus showing some discordance between protein and mRNA, a phenomena that is not uncommon and has been described before.[16] Collectively, the data indicate major dysregulation to integrin signaling and focal adhesion dynamics in BSM.

Conversion of BSM From a Contractile to a Synthetic Phenotype

To understand which biological and cellular pathways were up- or down-regulated by the loss of β1-integrin, we performed qPCR on a number of genes. Figure 8 shows those that broadly fall into 2 categories: ECM (Figure 8A) and interstitial and fibrosis markers (Figure 8B). The data represent quantitation of

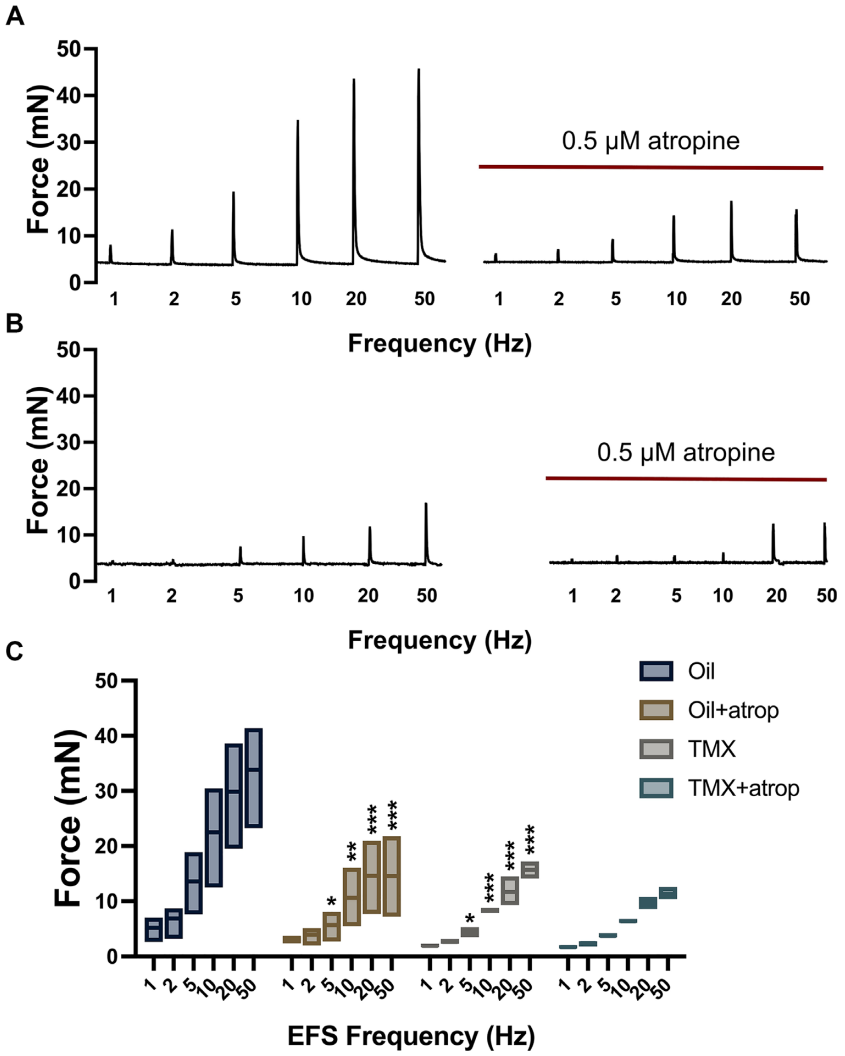

Figure 5. Muscle strip myography 6 wk after induction showing contraction force following EFS at different frequencies. (A) EFS on a muscle strip from an oil-injected mouse (left), and effect of atropine on that muscle (right). (B) EFS responses on muscle strip from a TMX-injected mouse (left) and effect of atropine on that strip (right). (C) Summary data are shown as mean and max–min range, $n = 3$–4 strips/bladder from 4 mice/group. Statistical analysis with multiple comparisons was done by 2-way ANOVA with Tukey's multiple comparisons testing. $*$ $P < 0.05$, $**$ $P < 0.01$, $***$ $P < 0.001$. Where significance is indicated the comparisons are with the "oil" control group. The "TMX+atrop" data were compared with "TMX" and were not significantly different at any frequency.

mRNA extracted from urothelium-stripped bladders of 4 oil-injected Myh11$^{\beta 1\text{-}fl/fl}$and 4 TMX-injected Myh11$^{\beta 1\text{-}fl/fl}$ mice at 6 wk postinjection. Somewhat surprisingly there were few detectable changes in expression of major matrix proteins with the exception of collagen III. An examination of interstitial markers (Figure 8B) revealed several interesting findings, including robust up-regulation of fibroblast-specific protein 1 (FSP1) and down-regulation of ectonucleoside triphosphate diphosphohydrolase 2 (NTPD2), a marker of interstitial cells that tend to wrap around BSM muscle bundles and are present deep in the lamina propria adjacent to the SM.[17] These would suggest the possible expansion of fibroblasts and with it the ability to lay down additional ECM (consistent with the Masson trichrome staining), while the NTPD2 population may be diminishing or phenoconverting. The lack of change in Hif1α, Tgfβ, and Ccn2 suggests the tissue is neither hypoxic nor experiencing inflammation,[18] while the lack of change in ki67 indicates that cells in the BSM are not proliferating. On balance, the picture presented suggests that myocytes in BSM are undergoing a phenotypic transition away from a contractile state to one that is more synthetic.

Discussion

Transmembrane integrin receptors are central to the mechanotranduction process because they both organize a cytoskeletal signaling complex within focal adhesions and preferentially focus tractional forces at these sites. Appropriate intracellular signaling arising from physical distortion of tissue during stretch and contraction forces during voiding require participation of both the ECM and the tensional network of the internal cytoskeleton. Force development is not possible without cell anchoring both internally and externally[2]. As that anchoring is dynamically regulated and fine-tuned constantly by integrins, it led us to hypothesize that they are likely to be critical to healthy functioning of the detrusor in the urinary bladder.

We recently showed that β1-integrin is rapidly upregulated in a mouse model of AUR[8] and others showed similar findings in a rat model of bladder stretch-injury.[15] More broadly, integrin signaling pathways have been shown to be dysregulated in neuropathic bladder[19,20] and diabetic bladder dysfunction.[21] Therefore, to explore the role of integrins in a more targeted

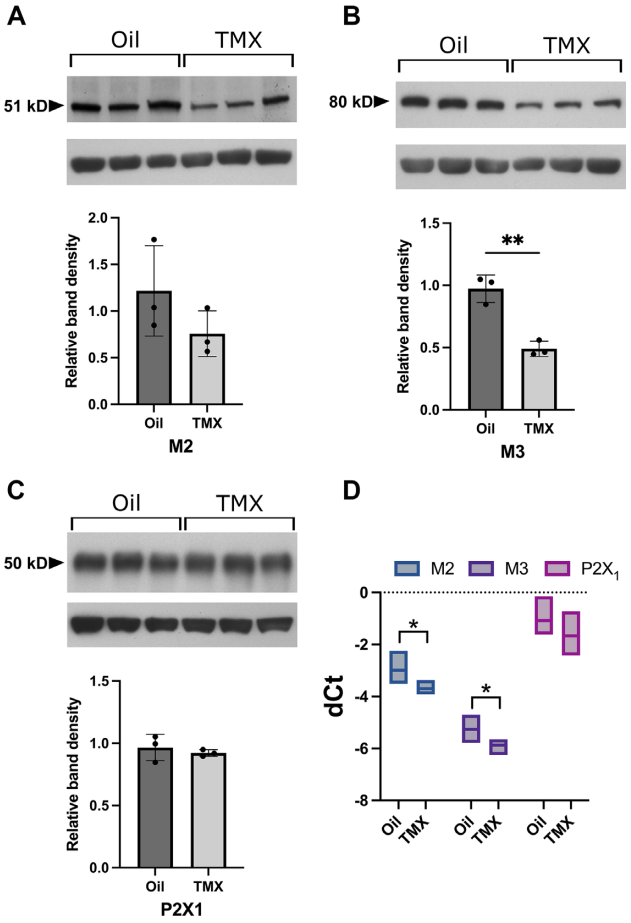

Figure 6. Western blotting on primary neurotransmitter receptors in BSM. (A) Muscarinic acetylcholine receptor 2 (M2), (B) muscarinic acetylcholine receptor 3 (M3), and (C) purinergic receptor P_2X1. Upper blots show the respective antibody binding to M3, M2, and $P2X_1$, while the lower blots show beta-actin staining. Quantitation by densitometry is shown beneath with receptor signals normalized to actin. Data are mean ± SD (D) qPCR data on all three receptors showing delta Ct values for mRNA extracted from 4 mice/group. Bars are mean and max–min range. $*$ $P < 0.05$, $**$ $P < 0.01$ by unpaired 2-tailed t-test.

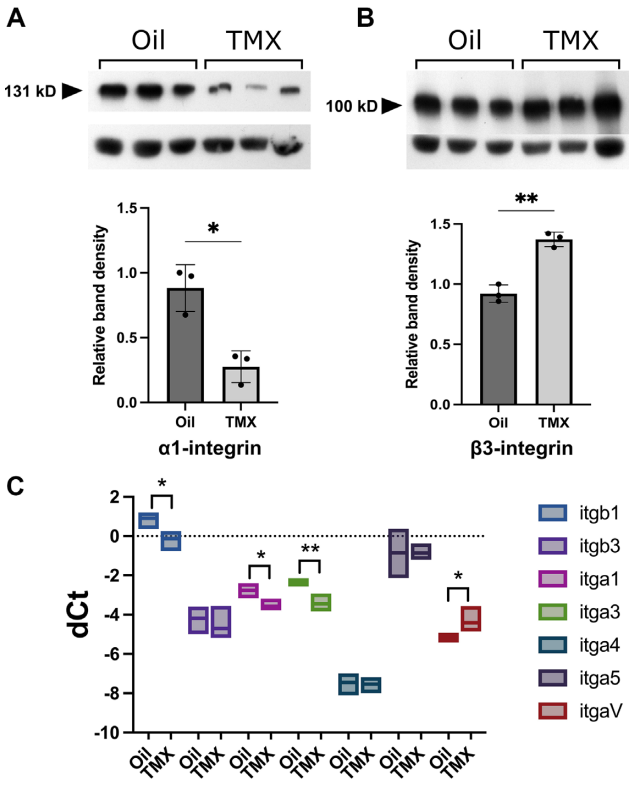

Figure 7. Western blotting and qPCR on other integrins in BSM. (A) α1-integrin and (B) β3-integrin. Upper panels show specific antibody binding to vehicle (oil) and TMX-treated mice at 56 days. Beta actin staining is below. Quantitation was by densitometry normalized to actin. Data are mean ± SD (C) qPCR on other integrin isoforms known to be expressed in bladder, showing delta Ct values for mRNA extracted from 4 mice/group. Bars are mean and max–min range. $*$ $P < 0.05$, $**$ $P < 0.01$ by unpaired 2-tailed t-test.

manner, we created a tissue-conditional and inducible knockout ($Myh11^{\beta1\text{-}fl/fl}$) to delete the major mechanosensory integrin in the BSM of adult mice. Experiments confirmed that >90% of β1-integrin protein was gone, 6 wk after a 1-wk regimen of TMX injections. This loss also resulted in down-regulation of α1- and α3-integrins, two of the most highly expressed alpha subunits in BSM, while β3-integrin protein was elevated, possibly in compensation (Figure 7). Turlo et al. studied a different SM knockout of β1-integrin and they also showed elevated β3-integrin in bladder and intestine.[22] Integrin αV in our model was also significantly upregulated, which is intriguing, since $\alpha V\beta3$ integrin was specifically shown to be associated with SM proliferation and SM phenotypic modulation in models of atherosclerosis.[23,24]

Unlike skeletal and cardiac muscle cells, which are terminally differentiated, mature SM cells retain an ability to undergo large-scale phenotypic conversion in response to genetic and environmental factors.[25,26] Physical forces experienced by SM affect gene expression and can radically alter cell differentiation.[27–30] Perturbation through altered physical and inflammatory stimuli, for example, plaque formation in large arteries, or airway obstruction in emphysema or asthma, causes the SM to phenoconvert from a physiologically quiescent contractile state to one that becomes pathologically activated and synthetic.[31–33] Phenoconversion can occur when the mechanical cues received are abnormal and sustained, leading to long term cell fate decisions involving dedifferentiation, proliferation, and migration.

This phenotypic plasticity is also important in chronic diseases of the bladder. There is now an awareness of the extensive remodeling of the bladder that can undergo in a number of settings, and how such remodeling is almost always accompanied by voiding impairment. Remodeling is seen in a number of prevalent conditions, including neurogenic bladder and outlet obstruction.[34–36] In a systematic review of studies of human bladder, outlet obstruction[37] common themes noted included early-stage hypertrophy of detrusor SM myocytes, followed at later stages by increases in connective tissue:SM ratio, which correlated with urodynamic findings such as reduced bladder compliance and increased post-void residual volume. Bladder dysfunction and remodeling also occurs with high prevalence in diabetes.[38,39] Mechanistically, however, the sequence of changes that occur during bladder remodeling is poorly understood and therefore difficult to halt or reverse.

There were several profound changes seen in both form and function of the bladder after the loss of β1-integrin. Histologically, there was an increase in the content of collagenous ECM and disrupted muscle bundle architecture (Figure 2) indicating the conversion of cells within the BSM toward a more synthetic phenotype. NTPD2 is a marker of an interstitial cell subpopulation located adjacent to BSM and also intercalated within

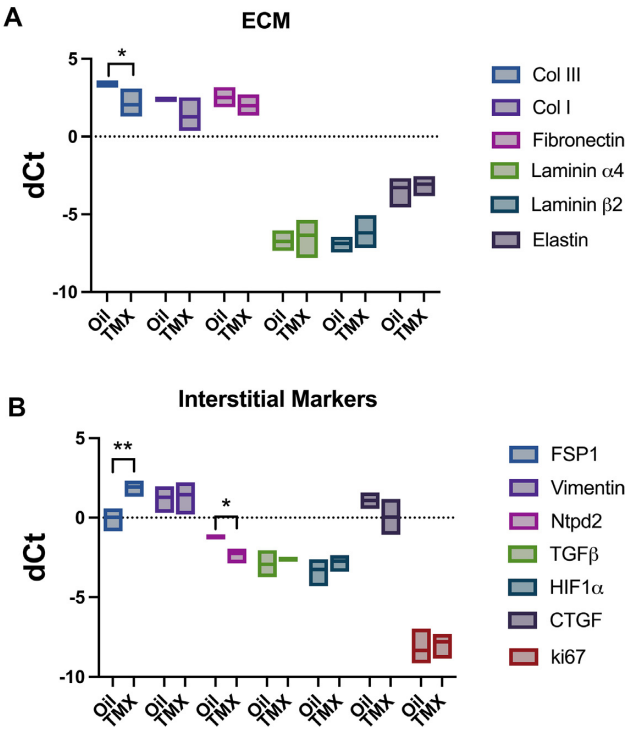

Figure 8. qPCR on genes related to (A) ECM and (B) interstitium, showing delta Ct values for mRNA extracted from 4 mice/group. Bars are mean and max–min range. $* P < 0.05$, $** P < 0.01$ by unpaired 2-tailed *t*-test. Gene nomenclatures are: Col III (Col 3a1), Col 1 (Col1a2), Fibronectin (Fn1), Laminin α4 (Lama4), Laminin β2 (Lamb2), Elastin (Eln), FSP (S100A4), Vimentin (Vim), CTGF (connective tissue growth factor, Ccn2), and ki67 (Mki67).

it, where it wraps around SM bundles.[17,40] Its downregulation suggests a loss of these cells as the BSM remodeled. The origin of the newly deposited matrix is unclear but the elevated transcriptional expression of fibroblast-specific protein 1 (FSP1, aka S100A4) may indicate a population of activated fibroblasts or myofibroblasts. Alternatively, myocytes may have phenoconverted from a contractile state to a biosynthetic one resembling myofibroblasts. Despite the name, FSP1 is expressed by a number of other cell types, including macrophages, lymphocytes, and myeloid cells,[41] and indeed by SM.[42] In a number of inflammatory settings, it is secreted, and once present in the extracellular microenvironment, it can act as a damage-associated molecular pattern and in this capacity has been implicated as a key player in both fibrosis[41,43] and SM phenoconversion.[44] Despite the clear accumulation of additional ECM, qPCR analysis indicated that classical markers of fibrosis (vimentin, TGFβ1, HIF1α, and CTGF) were not elevated. This was somewhat surprising but suggests that a phenotypic conversion of SM occurs that is unrelated to inflammation and pathological fibrosis. As such it speaks to the potency of integrin signaling in maintaining normal SM homeostasis. Future experiments using single cell transcriptomics (scRNA-seq) could answer important questions regarding the origins of FSP1 and the newly synthesized ECM.

Although transcription of β1-integrin is eliminated by Cre induction, the half-life of existing protein becomes key to the onset of functional impairment. The progressing nature of the phenotype can be seen in the void spot data (Figure 3). Serial measurements of voiding behavior in the same groups of awake unrestrained mice revealed an early phase response at day 18, in which the average volume/PV increased 2-fold. This is likely to be an accommodation response by the bladder to increased overall production of urine. Over time, however, the average voided volume diminished but the number of voids and hence the frequency increased. Cystometry confirmed increased frequency and further revealed that the bladder had weaker contractions and that both tone and compliance were impaired. These could be due to inappropriate mechanosensation leading to a failure to stimulate relaxation pathways during filling. The phenomenology is likely to be multifactorial however, since we assume that with matrix remodeling in the bladder wall, the mechanical stiffness is also altered.

To investigate the apparent loss of contraction force during voiding, we did muscle strip myography. These experiments confirmed a dramatic reduction in electrical field stimulated contraction force in the TMX-induced mice, and additional pharmacology revealed that the loss was almost completely due to reduced muscarinic responsiveness, with purinergic contractility relatively unaffected. Western blotting confirmed there was a significant loss of M3 receptor, the primary functional acetylcholine receptor in BSM responsible for contractility.[14] Consistent with the muscle strip pharmacology, $P2X_1$ levels were unaltered. These data collectively point to a specific regulatory interaction between β1-integrin and M2/M3 acetylcholine receptors.

It is clear from an extensive literature developed mainly in airway SM that the muscarinic signaling from acetylcholine leads to contraction in a manner that requires actin rearrangements, integrin engagement, and downstream integrin signaling.[45–53] Indeed the mechanism appears to be widely conserved as integrins have been shown to be necessary for SM contraction in multiple organs. Kim et al., for example, showed that carbachol treatment of bovine tracheal SM stimulated the recruitment of integrin-binding protein alpha-actinin to the plasma membrane,[46] a finding supported by and expanded upon by Zhang and Gunst.[51] In their study, stimulation of canine tracheal SM with acetylcholine increased the localization of alpha-actinin at the membrane and the amount of β1-integrin that coprecipitated with it. Furthermore, expression of an inhibitory integrin-binding peptide reduced contraction in response to acetylcholine, suggesting that recruitment of alpha-actinin to integrin complexes is necessary for tension development in SM. In renal vascular SM, it was shown that preincubating microperfused afferent arterioles with an integrin-specific binding peptide inhibited pressure-induced myogenic constriction,[54] while in human prostate SM, inhibiting $\alpha 2\beta 1$ integrin pharmacologically in organ bath experiments, inhibited neurogenic contraction by EFS as well as by thromboxane A2.[55] What has not been shown before is that the loss of integrin signaling drives a specific downregulation of M2/M3 receptor expression. The application of force to SM normally leads to rapid clustering of integrins and formation of expanded focal adhesions. These platforms, in turn, bring G-protein coupled receptors like M2 and M3 into close physical proximity and regulate their activity and downstream signaling. Without focal adhesions to organize them, it appears that expression of M2 and M3 is downregulated and the SM loses responsiveness to contractile stimuli.

Abnormal bladder contractility is a hallmark of several clinically important conditions. Detrusor overactivity (DO) is defined as a urodynamic observation characterized by involuntary detrusor contractions during the filling phase that may be spontaneous or provoked and result in frequency and urgency. It may or may not result in incontinence and first line treatment involves the use of anticholinergics in an effort to quieten contractility. Detrusor underactivity (DU) appears to represent

the opposite symptomatic presentation with low flow rates and inefficient emptying. The causes are poorly defined, but at least in a subset, they probably have a myogenic origin. In some conditions, such as diabetic cystopathy and benign prostatic hyperplasia, the bladder initially exhibits DO and then progresses to DU as the bladder decompensates. The role of integrins as either promotive of or responsive to these physical stresses is currently understudied, but the phenomenology highlighted here upon the loss of integrin signaling is very similar to certain clinical presentations.

It is tempting to speculate that the loss of appropriate mechanosensation results in a tissue that reorients to a markedly different compensatory response that disincentivizes contraction due to an inability to reorganize the cytoskeleton to generate additional anchoring and force transmission. As a further example of how muscarinic contraction, focal adhesion formation, and ECM are interconnected, it was shown in airway SM that addition of exogenous elastase (to alter ECM), modified muscarinic responses, and disrupted focal adhesion assembly dynamics.[56] In vitro experiments have also shown that ECM proteins differentially regulate airway SM phenotype and function.[57]

In sum we have demonstrated a critical role for integrin signaling in BSM in terms of its overall mechanobiology. The bladders in the knockouts continued to function, although in a highly dysregulated manner. The spectrum of effects noted, that is, the loss of muscarinic contractility, the excessive deposition of ECM, and the overactive phenotype exhibited, are highly reminiscent of a number of bladder pathologies that encompass neurogenic, metabolic, and incontinent phenotypes. Although speculative, it is possible that a unifying hypothesis for a number of these LUTS is that inappropriate physical stresses resulting in compensatory integrin-mediated mechanosensory responses by SM, which lead to biochemical sequelae that render both form and function altered in chronic settings.

Funding

None declared.

Acknowledgments

The authors wish to thank the Harvard Summer Research Program in Kidney Medicine (https://hskp.bwh.harvard.edu/) funded by a grant from NIDDK for the participation of summer students Sarah Z. Hanif and Erica M. Bien.

Conflicts of Interest

The authors have no conflicts of interest to disclose.

Data Availability

The data underlying this article will be shared on reasonable request to the corresponding author.

References

1. Ross TD, Coon BG, Yun S, et al. Integrins in mechanotransduction. *Curr Opin Cell Biol*. 2013;**25**(5):613–618. 10.1016/j.ceb.2013.05.006
2. Bachmann M, Kukkurainen S, Hytönen VP, Wehrle-Haller B. Cell adhesion by integrins. *Physiol Rev*. 2019;**99**(4): 1655–1699.
3. Hou XH, Hyun M, Taranda J, et al. Central control circuit for context-dependent micturition. *Cell*. 2016;**167**(1):73–86.10.1016/j.cell.2016.08.073
4. Verstegen AMJ, Klymko N, Zhu L, et al. Non-Crh glutamatergic neurons in Barrington's nucleus control micturition via glutamatergic afferents from the midbrain and hypothalamus. *Curr Biol*. 2019;**29**(17):2775–2789.10.1016/j.cub.2019.07.009
5. Coyne KS, Sexton CC, Thompson CL, et al. The prevalence of lower urinary tract symptoms (LUTS) in the USA, the UK and Sweden: results from the Epidemiology of LUTS (EpiLUTS) study. *BJU Int*. 2009;**104**(3):352–360.10.1111/j.1464-410X.2009.08427.x
6. Irwin DE, Kopp ZS, Agatep B, Milsom I, Abrams P. Worldwide prevalence estimates of lower urinary tract symptoms, overactive bladder, urinary incontinence and bladder outlet obstruction. *BJU Int*. 2011;**108**(7):1132–1138.
7. Natalin R, Lorenzetti F, Dambros M. Management of OAB in those over age 65. *Curr Urol Rep*. 2013;**14**(5):379–385.
8. Xie X, Chen H, Zhang L, et al. Molecular mechanisms of voiding dysfunction in a novel mouse model of acute urinary retention. *FASEB J*. 2021;**35**(4):e21447.
9. Truett GE, Heeger P, Mynatt RL, Truett AA, Walker JA, Warman ML. Preparation of PCR-quality mouse genomic DNA with hot sodium hydroxide and tris (HotSHOT). *BioTechniques*. 2000;**29**(1):52–54.10.2144/00291bm09
10. Hao Y, Wang L, Chen H, et al. Targetable purinergic receptors P2Y12 and A2b antagonistically regulate bladder function. *JCI Insight*. 2019;**4**(16):e122112.
11. Kim AK, Hamadani C, Zeidel ML, Hill WG. Urological complications of obesity and diabetes in males and females of three mouse models: temporal manifestations. *Am J Physiol Renal Physiol*. 2020;**318**(1):F160–F174.10.1152/ajprenal.00207.2019
12. Michel MC, Murphy TJ, Motulsky HJ. New author guidelines for displaying data and reporting data analysis and statistical methods in experimental biology. *Mol Pharmacol*. 2020;**97**(1):49–60.
13. Rajandram R, Ong TA, Razack AH, MacIver B, Zeidel M, Yu W. Intact urothelial barrier function in a mouse model of ketamine-induced voiding dysfunction. *Am J Physiol Renal Physiol*. 2016;**310**(9):F885–F894.
14. Giglio D, Tobin G. Muscarinic receptor subtypes in the lower urinary tract. *Pharmacology*. 2009;**83**(5): 259–269.
15. Upadhyay J, Aitken KJ, Damdar C, Bolduc S, Bagli DJ. Integrins expressed with bladder extracellular matrix after stretch injury in vivo mediate bladder smooth muscle cell growth in vitro. *J Urol*. 2003;**169**(2):750–755.
16. Payne SH. The utility of protein and mRNA correlation. *Trends Biochem Sci*. 2015;**40**(1):1–3.
17. Yu W, Zeidel ML, Hill WG. Cellular expression profile for interstitial cells of cajal in bladder—a cell often misidentified as myocyte or myofibroblast. *PLoS One*. 2012;**7**(11):e48897.10.1371/journal.pone.0048897
18. Tejera-Muñoz A, Marquez-Exposito L, Tejedor-Santamaría L, et al. CCN2 increases TGF-β receptor type II expression in vascular smooth muscle cells: essential role of CCN2 in the TGF-β pathway regulation. *Int J Mol Sci*. 2021;**23**(1):375.10.3390/ijms23010375

19. Dozmorov MG, Kropp BP, Hurst RE, Cheng EY, Lin HK. Differentially expressed gene networks in cultured smooth muscle cells from normal and neuropathic bladder. *J Smooth Muscle Res*. 2007;**43**(2):55–72.
20. Hipp JA, Hipp JD, Yoo JJ, Atala A, Andersson KE. Microarray analysis of bladder smooth muscle from patients with myelomeningocele. *BJU Int*. 2008;**102**(6):741–746.
21. Yohannes E, Chang J, Christ GJ, Davies KP, Chance MR. Proteomics analysis identifies molecular targets related to diabetes mellitus-associated bladder dysfunction. *Mol Cell Proteomics*. 2008;**7**(7):1270–1285.
22. Turlo KA, Scapa J, Bagher P, et al. β1-integrin is essential for vasoregulation and smooth muscle survival in vivo. *Arterioscler Thromb Vasc Biol*. 2013;**33**(10):2325–2335.
23. Blindt R, Krott N, Hanrath P, vom Dahl J, van Eys G, Bosserhoff AK. Expression patterns of integrins on quiescent and invasive smooth muscle cells and impact on cell locomotion. *J Mol Cell Cardiol*. 2002;**34**(12):1633–1644.
24. Ishigaki T, Imanaka-Yoshida K, Shimojo N, Matsushima S, Taki W, Yoshida T. Tenascin-C enhances crosstalk signaling of integrin αvβ3/PDGFR-β complex by SRC recruitment promoting PDGF-induced proliferation and migration in smooth muscle cells. *J Cell Physiol*. 2011;**226**(10):2617–2624.
25. Basatemur GL, Jørgensen HF, Clarke MCH, Bennett MR, Mallat Z. Vascular smooth muscle cells in atherosclerosis. *Nat Rev Cardiol*. 2019;**16**(12):727–744.
26. Halayko AJ, Amrani Y. Mechanisms of inflammation-mediated airway smooth muscle plasticity and airways remodeling in asthma. *Respir Physiol Neurobiol*. 2003;**137**(2-3):209–222.
27. Jensen LF, Bentzon JF, Albarrán-Juárez J. The phenotypic responses of vascular smooth muscle cells exposed to mechanical cues. *Cells*. 2021;**10**(9):2209.10.3390/cells10092209
28. Lacolley P, Regnault V, Segers P, Laurent S. Vascular smooth muscle cells and arterial stiffening: relevance in development, aging, and disease. *Physiol Rev*. 2017;**97**(4):1555–1617.
29. Safar ME, Nilsson PM, Blacher J, Mimran A. Pulse pressure, arterial stiffness, and end-organ damage. *Curr Hypertens Rep*. 2012;**14**(4):339–344.
30. Seow CY, Solway J. Mechanical and structural plasticity. *Compr Physiol*. 2011;**1**(1):283–293.
31. Finney AC, Stokes KY, Pattillo CB, Orr AW. Integrin signaling in atherosclerosis. *Cell Mol Life Sci*. 2017;**74**(12):2263–2282.
32. Jain M, Chauhan AK. Role of integrins in modulating smooth muscle cell plasticity and vascular remodeling: from expression to therapeutic implications. *Cells*. 2022;**11**(4):646.10.3390/cells11040646
33. Teoh CM, Tan SS, Tran T. Integrins as therapeutic targets for respiratory diseases. *Curr Mol Med*. 2015;**15**(8):714–734.
34. Deveaud CM, Macarak EJ, Kucich U, Ewalt DH, Abrams WR, Howard PS. Molecular analysis of collagens in bladder fibrosis. *J Urol*. 1998;**160**(4):1518–1527.
35. Haferkamp A, Dörsam J, Resnick NM, Yalla SV, Elbadawi A. Structural basis of neurogenic bladder dysfunction. II. Myogenic basis of detrusor hyperreflexia. *J Urol*. 2003;**169**(2):547–554.
36. Ito S, Nomura T, Ueda T, et al. Gene expression profiles during tissue remodeling following bladder outlet obstruction. *Sci Rep*. 2021;**11**(1):13171.
37. Fusco F, Creta M, De Nunzio C, et al. Progressive bladder remodeling due to bladder outlet obstruction: a systematic review of morphological and molecular evidences in humans. *BMC Urology*. 2018;**18**(1):15.
38. Lee WC, Wu HP, Tai TY, Liu SP, Chen J, Yu HJ. Effects of diabetes on female voiding behavior. *J Urol*. 2004;**172**(3):989–992.
39. Lifford KL, Curhan GC, Hu FB, Barbieri RL, Grodstein F. Type 2 diabetes mellitus and risk of developing urinary incontinence. *J Am Geriatr Soc*. 2005;**53**(11):1851–1857.
40. Yu W, Robson SC, Hill WG. Expression and distribution of ectonucleotidases in mouse urinary bladder. *PLoS One*. 2011;**6**(4):e18704.
41. Li Z, Li Y, Liu S, Qin Z. Extracellular S100A4 as a key player in fibrotic diseases. *J Cell Mol Med*. 2020;**24**(11):5973–5983.
42. Brisset AC, Hao H, Camenzind E, et al. Intimal smooth muscle cells of porcine and human coronary artery express S100A4, a marker of the rhomboid phenotype in vitro. *Circ Res*. 2007;**100**(7):1055–1062.
43. Wu Y, Zhang W, Gunst SJ. S100A4 is secreted by airway smooth muscle tissues and activates inflammatory signaling pathways via receptors for advanced glycation end products. *Am J Physiol Lung Cell Mol Physiol*. 2020;**319**(1):L185–L195.
44. Chaabane C, Heizmann CW, Bochaton-Piallat ML. Extracellular S100A4 induces smooth muscle cell phenotypic transition mediated by RAGE. *Biochim Biophys Acta - Mol Cell Res*. 2015;**1853**(9):2144–2157. 10.1016/j.bbamcr.2014.07.022
45. Huang Y, Zhang W, Gunst SJ. Activation of vinculin induced by cholinergic stimulation regulates contraction of tracheal smooth muscle tissue. *J Biol Chem*. 2011;**286**(5):3630–3644.
46. Kim HR, Hoque M, Hai CM. Cholinergic receptor-mediated differential cytoskeletal recruitment of actin- and integrin-binding proteins in intact airway smooth muscle. *Am J Physiol Cell Physiol*. 2004;**287**(5):C1375–C1383.10.1152/ajpcell.00100.2004
47. Kim HR, Liu K, Roberts TJ, Hai CM. Length-dependent modulation of cytoskeletal remodeling and mechanical energetics in airway smooth muscle. *Am J Respir Cell Mol Biol*. 2011;**44**(6):888–897.
48. Mahavadi S, Grider JR, Murthy KS. Muscarinic m2 receptor-mediated actin polymerization via PI3 kinase γ and integrin-linked kinase in gastric smooth muscle. *Neurogastroenterol Motil*. 2019;**31**(2):e13495.
49. Opazo Saez A, Zhang W, Wu Y, Turner CE, Tang DD, Gunst SJ. Tension development during contractile stimulation of smooth muscle requires recruitment of paxillin and vinculin to the membrane. *Am J Physiol-Cell Physiol*. 2004;**286**(2):C433–C447.10.1152/ajpcell.00030.2003
50. Paredes-Gamero EJ, Medeiros VP, Farias EH, et al. Heparin induces rat aorta relaxation via integrin-dependent activation of muscarinic M3 receptors. *Hypertension*. 2010;**56**(4):713–721.10.1161/hypertensionaha.110.156877
51. Zhang W, Gunst SJ. Dynamic association between alpha-actinin and beta-integrin regulates contraction of canine tracheal smooth muscle. *J Physiol*. 2006;**572**(3):659–676. 10.1113/jphysiol.2006.106518
52. Zhang W, Wu Y, Wu C, Gunst SJ. Integrin-linked kinase regulates N-WASp-mediated actin polymerization and tension development in tracheal smooth muscle. *J Biol Chem*. 2007;**282**(47):34568–34580. 10.1074/jbc.M704966200

53. Slack BE. Tyrosine phosphorylation of paxillin and focal adhesion kinase by activation of muscarinic m3 receptors is dependent on integrin engagement by the extracellular matrix. *Proc Natl Acad Sci*. 1998;**95**(13):7281–7286. 10.1073/pnas.95.13.7281
54. Balasubramanian L, Ahmed A, Lo CM, Sham JS, Yip KP. Integrin-mediated mechanotransduction in renal vascular smooth muscle cells: activation of calcium sparks. *Am J Physiol Regul Integr Comp Physiol*. 2007;**293**(4):R1586–R1594.10.1152/ajpregu.00025.2007
55. Li B, Wang X, Wang R, et al. Inhibition of neurogenic and thromboxane A_2-induced human prostate smooth muscle contraction by the integrin $\alpha 2\beta 1$ inhibitor BTT-3033 and the integrin-linked kinase inhibitor Cpd22. *Prostate*. 2020;**80**(11):831–849. 10.1002/pros.23998
56. Lockett AD, Wu Y, Gunst SJ. Elastase alters contractility and promotes an inflammatory synthetic phenotype in airway smooth muscle tissues. *Am J Physiol Lung Cell Mol Physiol*. 2018;**314**(4):L626–L634.
57. Dekkers BG, Schaafsma D, Nelemans SA, Zaagsma J, Meurs H. Extracellular matrix proteins differentially regulate airway smooth muscle phenotype and function. *Am J Physiol Lung Cell Mol Physiol*. 2007;**292**(6):L1405–L1413. 10.1152/ajplung.00331.2006